PERIODICA POLYTECHNICA SER. MECH. ENG. VOL. 41, NO. 1, PP. 55-67 (1997)

IMPLEMENTATION OF THE PUSH-OUT TEST FOR IMPROVING OF COMPOSITE INSULATOR END FITTING PERFORMANCE

Oleg I. BENEVOLENSKY* – György KRALLICS* – Victor S. KLEKOVKIN**

*Institute for Mechanical Technology and Materials Science
Technical University of Budapest
H–1521, Budapest, Hungary
**Department of Robotics Systems
Izhevsk State Technical University
426069 Izhevsk, Udmurtia, Russia

Received: April 17, 1996

Abstract

Destructive push-out test of composite rod joint was prepared in order to estimate ultimate load capacity of composite insulators end fitting joint. Plane strain and axisymmetric finite element models were developed. Imperfect interface with large allowed slipping and Coulomb friction was analysed. Experimental results were preliminary processed and ultimate load criteria chosen for appropriate manipulation and comparison. Results show that composite joints with contact pressures higher than the radial strength do not obey Coulomb friction law due to partial damage effect on the composite rod surface. However, for joints with limited contact pressure good agreement with classical friction model was obtained. Generalised relation between ultimate axial stress and contact pressure was also presented.

Keywords: electrical composite insulator, Finite Element Analysis, cylindrical joint, load capacity.

1. Introduction

Glass reinforced polymers are replacing recently ceramic insulators in electrical High Voltage lines and other applications. They represent a number of advantages compared to conventional materials. These are high strength/weight ratio, flexibility, ease of installation and others [1]. A conventional composite insulator is shown in *Fig. 1.* It consists of core, weathersheds and metal end fitting. Compression fitted joints are produced by squeezing of metal armature, aluminium or ductile iron, generally. Presented interference fit is obtained due to work hardening phenomena in the steel end fitting. Since steel part demonstrates elastic-plastic behaviour after certain magnitude of applied load plastic strains are developing. When joint is unloaded residual plastic strains in outer part remain. It causes residual radial elastic stresses in both parts and Hertzian contact pressure upon the interface which is expected to be purely mechanical in nature

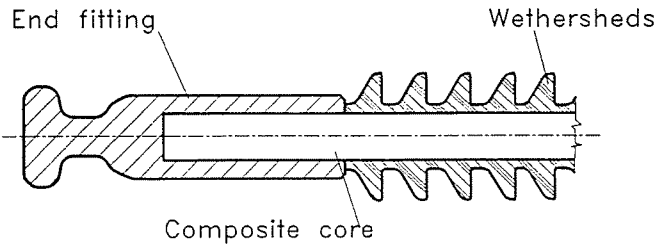

Fig. 1. Conventional composite insulator design

during the life time composite core subjected to tensile force pooling it out of the end fitting.

According to BANSAL et al. [1] and MIER-MAZA et al. [3] failure frequently occurs near to the fitting area. Therefore the end fitting design should be improved. The most important factors of joint capacity are the crimping process parameters. In order to evaluate the influence of these parameters on the joint's strength and accumulate more complete information about ultimate capacity of insulator joint and debonding process destructive push down test and Finite Element simulation were arranged.

2. Push-out Test Implementation

Schematic illustration of construction used for experiment is presented in *Fig. 2.* Given design allows to obtain complete understanding of debounding process using a simple experimental set up. The experimental equipment consists of ductile steel sleeve and composite rod cut. Sleeve of steel C45 demonstrates elastic plastic behaviour. Unidirectional E-glass/Epoxy composite rod has a longitudinal fibres alignment. Joint is obtained by crimping of steel sleeve upon the composite rod cut. Two types of sleeves are used. These are parts with 40 and 44 mm outer diameter. Experiment itself consists of crimping and push-out stages. During the push-out stage axial pushing load is applied to the rod edge. Axial displacement and axial force values are measured for a number of crimped specimens using MTS 810 testing machine.

3. Finite Element Simulation

A Finite Element model of the push-out test was developed to make evident the possibility of composite electrical insulator end fitting modelling.

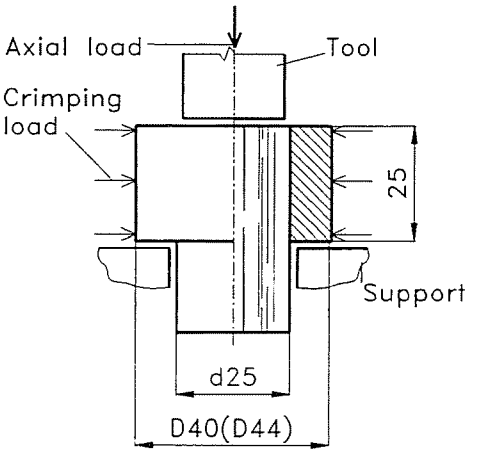

Fig. 2. Schematic illustration of the experimental rig

General purpose Finite Element code MARC 6.1 has been used for the end fitting joint simulation. A number of assumptions were accepted:

- composite rod is considered to be homogeneous due to big amount of fibres and random distribution in the matrix;
- composite rod is orthotropic and obeys to the Hook's law;
- end fitting is homogeneous, isotropic and demonstrates elastic-plastic behaviour according to isotropic hardening rule;
- dry Coulomb friction model is employed for simulation of the contact;
- displacements are to be large and strains to be small.

The constitutive equation for anisotropic linear elastic material is presented as

$$\sigma_{ij} = C_{ijkl}\varepsilon_{kl}\,. \tag{1}$$

The values of C_{ijkl} and the preferred directions must be defined for an anisotropic material. The orthotropic stress–strain relationship for a plain strain element can be described as

$$C = \frac{1}{(1-\nu_{12}\nu_{21})}\begin{bmatrix} E_1 & \nu_{21}E_1 & 0 \\ \nu_{12}E_2 & E_2 & 0 \\ 0 & 0 & (1-\nu_{12}\nu_{21})\,G \end{bmatrix}, \tag{2}$$

where $G = E_3/\left(2\left(1+\nu_{13}\right)\right)$ is the shear module.

The elastic-plastic material behaviour is governed by the von Mises yield criterion and the isotropic hardening rule. Numerical calculation is based on the incremental theory of plasticity. Von Mises Yield criterion

states that yield occurs when the equivalent von Mises stress ($\overline{\sigma}$) equals the yield stress (σ_s) measured from an uniaxial test. For an isotropic material

$$\overline{\sigma} = \sqrt{\frac{\left[(\sigma_1 - \sigma_2)^2 + (\sigma_2 - \sigma_3)^2 + (\sigma_3 - \sigma_1)^2\right]^{1/2}}{2}}, \tag{3}$$

where σ_1, σ_2 and σ_3 are the principal stresses.

Flow rule is represented by Prandtl–Reuss relation [8]

$$\mathrm{d}\varepsilon_{ij}^{ep} = \frac{1+\nu}{E}\mathrm{d}\sigma_{ij} - \frac{\dot{\nu}}{E}\delta_{ij}\mathrm{d}\sigma_{kk} + \frac{9}{4h}\frac{\sigma'_{ij}\sigma'_{kl}}{\overline{\sigma}^2}\mathrm{d}\sigma_{kl}\,, \tag{4}$$

where σ'_{ij} denotes the deviatoric stress, h is the strain hardening rate and δ_{ij} is the Kronecker delta (when $i = j$, $\delta_{ij} = 1$; when $i \neq 1$, $\delta_{ij} = 0$).

Imperfect interface between rod and sleeve was analysed, so that large relative sliding was allowed. Friction in contact was described by Coulomb's law (see at [7]) in form of

$$F_t \cdot \mathbf{t} \leq \mu F_n \mathbf{t}\,, \tag{5}$$

where F_n is the force normal to contact surface and F_t is the tangential force, μ denotes the friction coefficient and $\mathbf{t}$ is the unit vector in sliding direction.

E-glass/Epoxy composite rod has a glass volume fraction V_f of about 60%. Since recently it was intensively used for electrical substation application quite a big number of researchers presented analytical and experimental properties of this material. These data could be found in a number of works (see at [1, 3, 6]). Therefore material constants can be accepted upon the analysis of the existent data. These constants are given in *Table 1*.

Table 1
Material constants for E-glass/Epoxy of $V_f = 60\%$

Properties	E_{11} GPa	E_{22} GPa	G_{12} GPa	G_{23} GPa	σ_{22}^m MPa	ν_{12}	ν_{23}
Values	40	10	4.5	4.0	150	0.29	0.26

where 1 is the longitudinal direction and σ_{22}^m denotes transversal strength measured from compression test.

Work hardening curve for steel C45 is given in *Fig. 3* and defined by analytical relationship

$$\sigma_s = 687 + 650 \cdot (\varepsilon^p)^{0.4}\,, \tag{6}$$

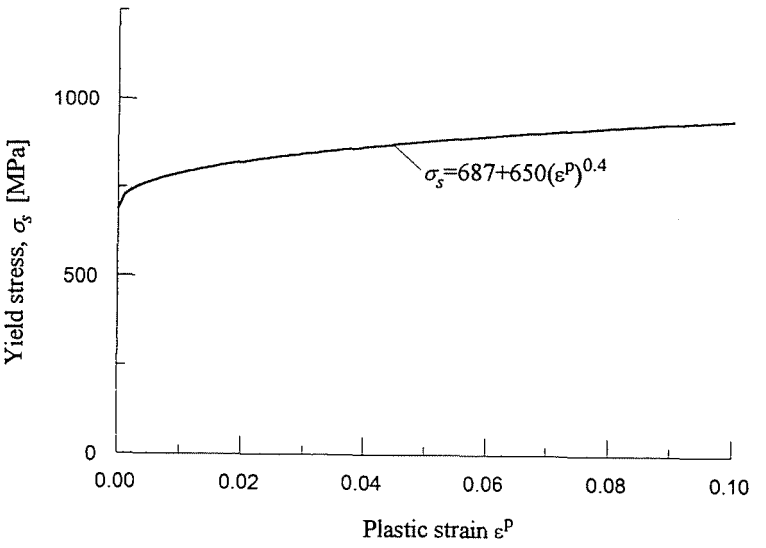

Fig. 3. Work hardening curve for steel C45

where ε^P is the plastic strain.

Definition of the friction coefficient was provided within conditions most close to the provided push-out test. Geometry, contact surface roughness and contact pressure value were chosen to be maximum alike to experimental. Friction coefficient was calculated using following formulation. Sleeve of 44 mm outer diameter was produced with the inner diameter d_{cyl} smaller than rod cut diameter d_r. It guarantied appearance of the contact pressure in the interface. Quality of the inner surface was obtained equal to samples used in push-out test. Initial sleeve outer diameter D_{ini} was precisely measured by Universal measuring microscope. After it rod cut was indented to the hole by means of a measuring testing machine. Maximum registered force during the *pushing down* represented the friction force. Elastic radial displacement of the sleeve was defined as half a difference between the *outer diameters* of assembled sleeve D_a and initial one D_{ini}

$$U_r = \frac{D_a - D_{ini}}{2}. \tag{7}$$

Simple Finite Element model for definition of contact pressure as a function of radial displacement was developed. It showed that these parameters are related by approximately linear equation

$$p = 10.14 \cdot 10^3 U_r\,. \tag{8}$$

Sliding friction coefficient was calculated as follows

$$\mu = \frac{F_t}{pS_{cyl}}, \tag{9}$$

where $S_{cyl} = \pi d_r H$ is the contact area,
H is the sleeve height.

Resulting value of $\mu = 0.3$ was accepted for further calculation even at higher contact loads.

Numerical simulation is developed in sequence according to technological steps of experiment. It consists of elastic-plastic crimping and pushing out processes simulation. General schema of the modelling procedure is presented in *Fig. 4*.

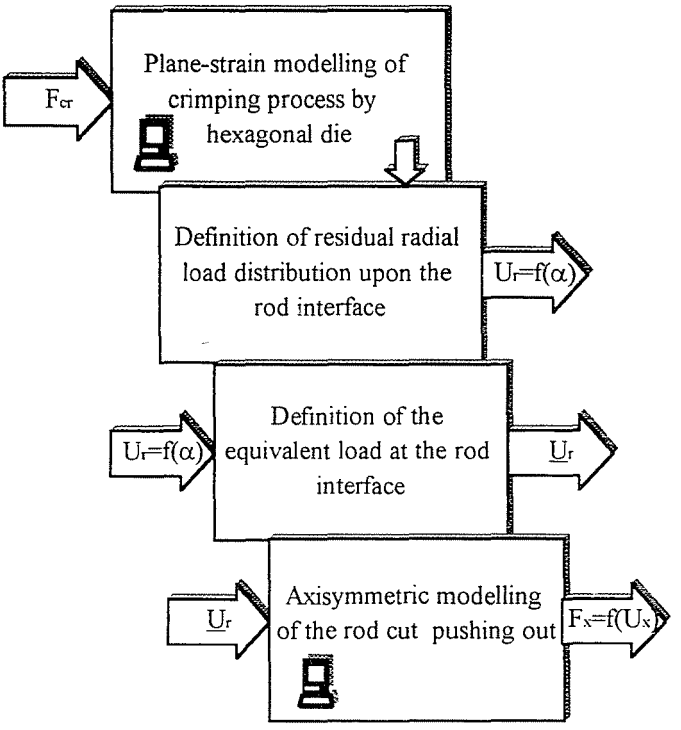

Fig. 4. General schema of the modelling procedure

For modelling of the elastic-plastic crimping process in the midplane a plain-strain FE model is used (see *Fig. 5*). Four and three node plain strain elements are used for simulation. Die is assumed to be much stiffer than

elastic-plastic sleeve. Geometry of the model corresponds to dimensions of the samples. The angle between the neighbouring die working surfaces equals to 120 degrees. Two different dies were modelled for samples of 40 and 44 mm diameters. As a result of numerical simulation distribution of residual contact loads is obtained for given crimping load value.

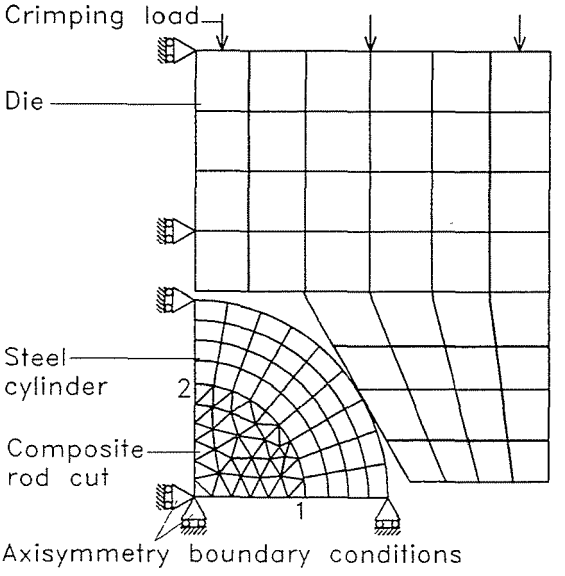

Fig. 5. Plane-strain FE model of the crimping process

Distribution of radial displacements U_r along **1 − 2** arc is shown in *Fig. 6*, where α denotes the angle between point **1**, the origin and a point of the interface. As a matter of fact, a hexagonal die is used to crimp the end fittings on to the composite rod. It causes wave-like distribution of radial displacements in circumferential direction of the interface. Crimping load of 575 kN causes plastic deformations just at the contact area near to $\pi/6$ (30 degrees). However, with the rising of crimping force die comes in contact near to $\alpha = \pi/2$ area also. Since the employed axisymmetric finite element model assumes uniform distribution of the radial load in the circumference a relationship between the actual displacement field in the *midplane* and the applied one for the axisymmetrical model should be defined, i.e. average residual radial displacement of the midplane rod bound $\underline{U}_r$ is calculated and is used for axisymmetric simulation further.

Axisymmetric finite element model of the push-out test is shown in *Fig. 7*. Since after unloading there are just elastic residual stresses in crimped steel sleeve it is assumed to be elastic in the axisymmetric model. Required contact pressure is obtained by the axial displacement applied

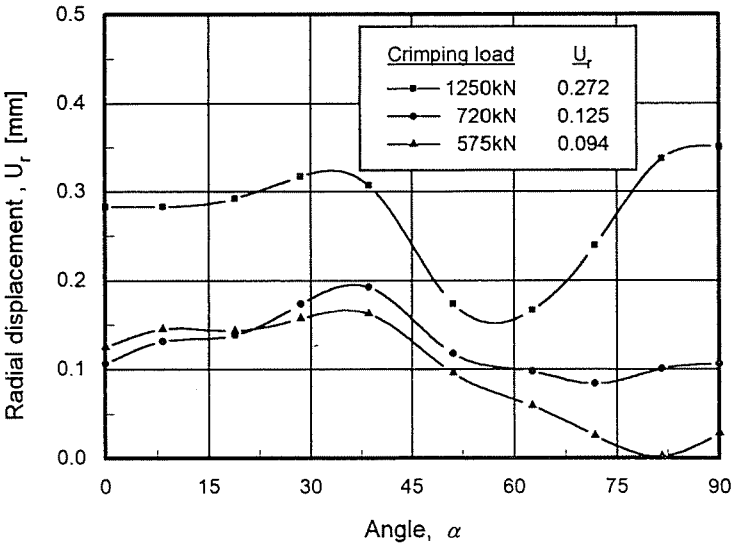

Fig. 6. Distribution of radial displacements along the interface

to sleeve bound. Numerical curves of pushing force versus axial displacement were calculated corresponding to different crimping force values. The complete push-out was simulated in order to define joint failure mode.

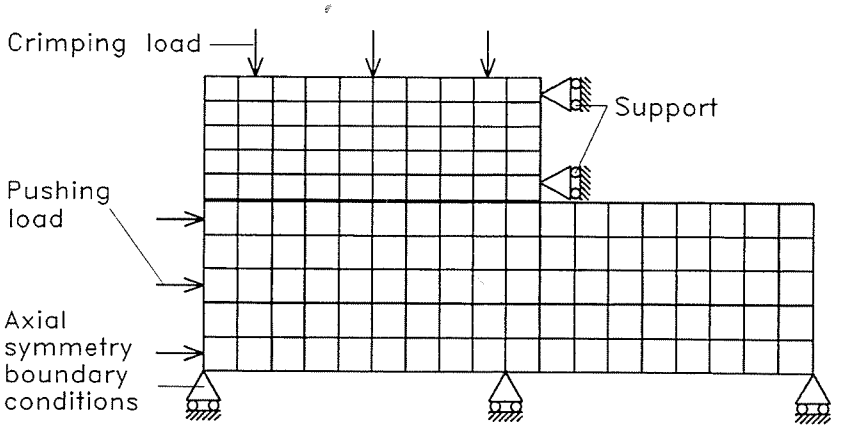

Fig. 7. Axisymmetric Finite Element model of the push-out test

4. Comparison of the Results

Axial load versus axial displacement experimental curves are given in *Fig. 8.* We admit that direct analysis of experimental data is complicated due to high non-linear behaviour and can be misleading at first. Let us consider D40 curve in more details. It refers to crimping force F_{cr} of 1300 kN and sleeve diameter of 40 mm. The curve consists of following typical parts:

0 – 1 linear (elastic response of system);
1 – 2 debounding process (gradual distribution of the sliding area);
2 – 3 joint failure (free sliding along whole contact surface);
3 – 4 sliding with the uniform sliding velocity distribution;
4 equilibrium of the applied load and friction force.

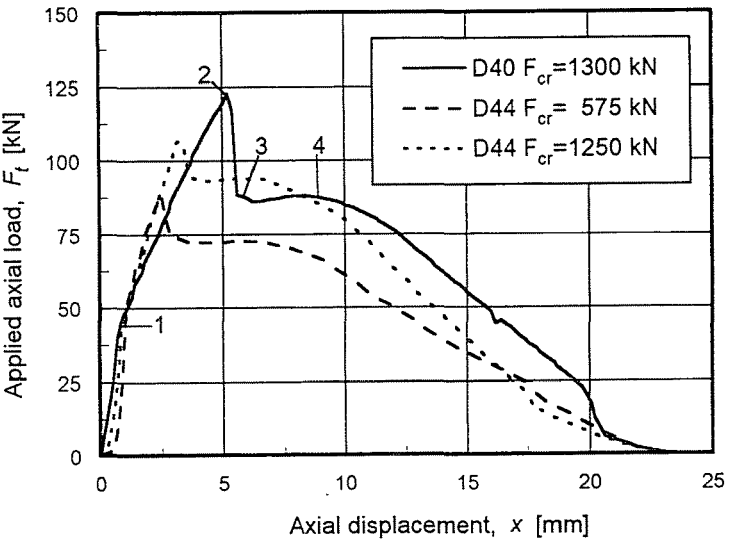

Fig. 8. Experimental results of the push-out test

Analysis of even a small quantity of experimental curves indicates that ultimate axial force measured in point 2 can be subjected to considerable fluctuation because system is not steady. Much more stable parameter is an axial load value in equilibrium with the friction force (point 4). This criterion expresses the ultimate tensile force and remains persevering for every curve. We will use it as a criterion of load bearing capacity further. However, equilibrium happens in time moment corresponding to different contact length (displacement x) and could hardly be compared with others.

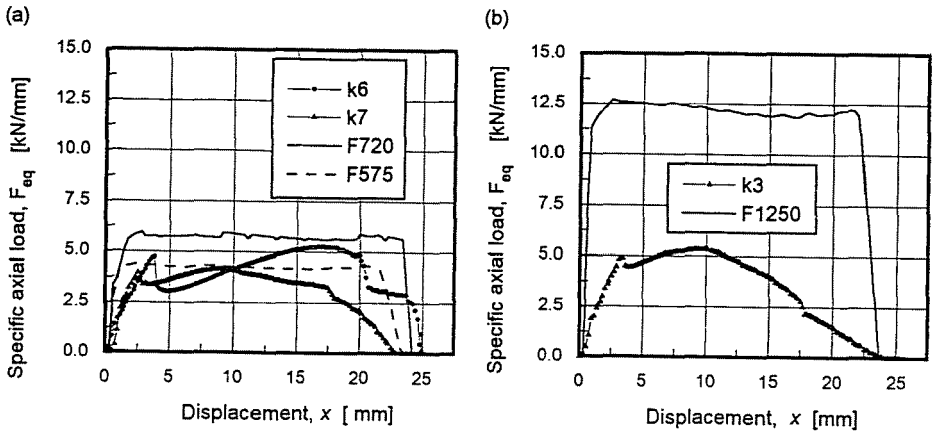

Fig. 9. Numerical and experimental results comparison. Crimping force $F_{cr} = 575\,\text{kN}$, $F_{cr} = 720\,\text{kN}$ *a*) and $F_{cr} = 1250\,\text{kN}$ *b*)

Expressing axial load as

$$F_t = \mu F_n = \mu p \pi d l = \mu p \pi d (L - x)\,, \tag{10}$$

where l is the current contact length, L denotes length of sleeve and x the axial current displacement, we get axial load as a function of variable x

$$F_t = F_t(x)\,, \tag{11}$$

where $x \in [0, L)$.

Dividing both parts of (11) by the $L - x$ we can obtain function F_{eq}.

$$F_{eq} = \frac{F_t(x)}{L - x} = \mu p \pi d\,. \tag{12}$$

Specific axial load F_{eq} does not depend of axial displacement directly any more and describes motion process assuming the contact length as unit and constant. Moreover, load values could be compared adequately. Since axial load is presented in relative units we are able to apply these results to a variety of joints geometry. Further we will use specific axial force default in order to operate uniformly with experimental and numerical results.

Numerical and experimental results of the push-out test for crimping force $F_{cr} = 575\,\text{kN}$ and $F_{cr} = 720\,\text{kN}$ (sleeve diameter of 44 mm) are given in *Fig. 9a*.

Numerical curves $F575$ and $F720$ rapidly climb from the very beginning and remain almost stable while bodies are in contact. It corresponds well to Coulomb friction implementation since friction load is constant with constant contact area. Inspite of that fact that *experimental curves* $k7$ and $k6$ (corresponding to crimping load of 575 kN and 720 kN, respectively) demonstrate large non-linearity they are rather close to numerical results in peaks. It validates load capacity criteria as an adequate one. However, results in *Fig. 9b* show considerable differences. Curve $k3$ refers to experimental results for crimping force of 1250 kN. This disagreement will be elaborated below.

In order to obtain more complete knowledge about the subject we generalise all obtained results in terms of contact pressure ratio (contact pressure/maximum radial stress) and axial stress. *Fig. 10* collects all these data. Curve T_1 shows theoretical axial stress versus contact pressure ratio for infinitely long pure Her-tzian contact with friction coefficient of 0.3. The numerical curve also presents linear relation but with smaller slope angle. It can be explained by the limited length of the sleeve and not uniform contact pressure distribution along the x axis. Quite good agreement of experimental and numerical results is observed in the first quarter. But with rising of the contact pressure disagreement increases.

Analysis of contact pressure ratio to maximum radial stress and investigation of the rod cuts after being pushed out from the sleeve showed that partial surface damage occurs due to high and unequal distributed radial stresses along the circumferential direction in the rod boundary. It means that Coulomb friction model cannot be used any more due to the rod surface that is not an ideal solid body surface.

Curve T_2 is employed in order to describe the character of actual load/pressure curve considering samples surfaces partly damaged. It indicates that beginning from contact pressure ratio of about 1.5 increasing of the contact load does not lead to significant increasing of the load bearing capacity on one hand and introduces damage onother hand.

Consideration of the wave-like contact loads distribution in circumference and much higher level of contact pressure before crimping loads had released brings more strict limitation on contact pressure value.

5. Conclusions

Results show clearly that analysis of contact problems of materials with extremely different mechanical properties must be executed carefully to avoid disagreement with actual contact conditions. However, FE simulation

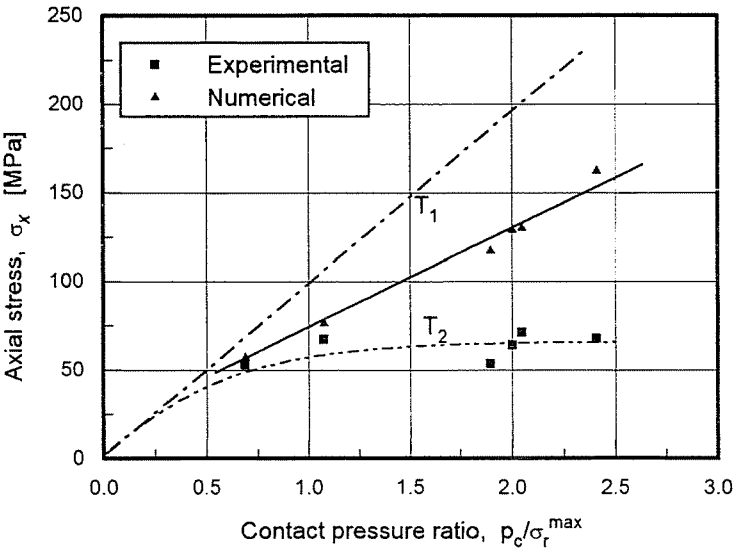

Fig. 10. Generalised results of the research

can be successfully employed for composite electrical insulators end fitting analysis considering reasonable contact pressure rate.

Highly unequal distribution of the radial loads along the circumference of the interface causes the local damage areas at the crimped rod. Locally damaged rod will have lower service characteristics during the long term period.

Wave-like distribution of the interface loads significantly decreases the available level of average contact pressure because it is limited by maximum values in peaks.

Acknowledgements

This research was primarily realised using equipment and software of the Institute of Mechanical Technology and Materials Science. Authors express their gratitude for the help and consulting of any kind to Levente TATÁR, Institute of Mechanical Technology and Materials Science, Mechanical Faculty, TUB. We are grateful also to Dr. Károly VÁRADY, Institute of Machine Design, TUB, for reading the manuscript and his remarks.

References

1. BANSAL, A. – SCHUBERT, A. – BALAKRISHMAN, M. V. – KUMOSA, M. (1995): Finite Element Analysis of Substation Composite Insulators. *Composite Science and Technology,* Vol. 55, pp. 375–389.
2. CHERNEY, E. A. (1991): Partial Discharge – Part V. PD in Polymer Type Line Insulators. *IEEE Electrical Insulation magazine,* No. 7, pp. 28–32.
3. MIER-MAZA, R. – LANTEIGNE, J. – DE TOURREIL, C. (1983): Failure Analysis of Synthetic Insulators with Fibreglass rod Submitted to Mechanical Loads. *IEEE Trans. Power Apparatus and Systems,* PAS-102, pp 3123–9.
4. PIGGOT. M. R. (1980): Load-Bearing Fibre Composites, Pergamon Press, Oxford.
5. HOLMES, M. – JUST, D. J. (1983): GRP in Structural Engineering, Applied Science Publisher.
6. KRISHAN, K. CHAWLA (1987): Composite Materials, Science and Engineering, Germany.
7. MARC K6.1 (1994): User Information, Marc Analysis Research Corporation, USA, Vol. A.
8. (1982): Numerical Methods in Industrial Forming Processes. (Ed. Pittman, J. F. T. et al., Pineridge Press, U.K. pp. 39–50.